SLAC-PUB-10018
June 2003

The Dynamic Response of Magnetization to Hot Spins

Wolfgang Weber[1], Stefan Riesen[1], and Hans C. Siegmann[2]

[1] Laboratorium für Festkörperphysik, ETH Zürich, 8093 Zürich, Switzerland
wolfgang.weber@ipmcs.u-strasbg.fr
[2] Stanford Linear Accelerator Center, Stanford University,
Stanford, CA 94309, USA

Abstract. When electrons interact with a ferromagnet, their spin polarization vector is expected to move, depending on the magnetization of the ferromagnetic material. This spin motion, consisting of an azimuthal precession and a polar rotation about the magnetization direction, is measured. The precession of the spin polarization vector generates a torque on magnetization that turns out to be large with low-energy electrons. This makes injection as well as reflection of spin-polarized electrons an attractive alternative concept for magnetization switching.

1 Introduction

If electrons interact with a ferromagnetic material, there is spin-dependent scattering as well as exchange interaction between the incident electrons and the electrons that establish the magnetization. In both processes, angular momentum is transferred from the incident electrons to the magnetization, leading to excitation of the magnetization [1,2,3]. By injecting electron currents of high density through nanocontacts, these excitations have been observed via the occurrence of spin waves, changes in the micromagnetic structure, and even switching of the magnetization [4,5,6,7,8]. All of these phenomena may occur together, and additionally, there may also be an effect of the magnetic field surrounding the injected beam of electrons [9]. Hence, it is difficult to interpret most of the current experiments in terms of specific elementary processes. To understand the details of the angular momentum transfer process, it is neccessary to get information about the torque exerted on the magnetization by the injected electrons. However, only very recently was it possible to determine this key quantity [10]. It has been shown that the torque exerted on magnetization by the injection of spin-polarized electrons can be determined experimentally without any further assumptions. This torque turns out to be surprisingly large and may be used to induce precessional magnetization reversal, leading to a new concept of writing magnetic bits in nanosized ferromagnets.

In Sect. 2, the absorption and spin motion of electrons interacting with thin ferromagnetic layers are discussed. Two types of motion of the spin-polarization vector occur: a precession about the magnetization direction

Work supported in part by the Department of Energy contract DE-AC03-76SF00515.
Submitted to Topics in Applied Physics

and a rotation into it. From this, the torque exerted on the incident electrons by magnetization is determined. By exploiting angular momentum conservation, we can then infer the torque exerted by the spin-polarized electrons on the magnetization (see Sect. 3). It is of the same magnitude but opposite direction. This torque leads to significant precession of magnetization at experimental current densities. In nanocontacts with radii below 100 nm, this exchange-induced precession is larger compared to the precession induced by the regular magnetic field of the current. Therefore, precessional magnetization reversal by injection or reflection of spin-polarized electrons is the method of choice for reversing the magnetization in magnetic bits such as used in magnetic random access memories, for instance. In fact, it is proposed to exploit technologically the huge exchange fields in ferromagnetic materials to switch magnetization.

2 Absorption and Spin Motion of Electrons in Ferromagnets

The discovery of giant magnetoresistance [11] has opened a new field of research, the spin-dependent transport of conduction electrons at the Fermi level, and has triggered numerous studies in the last decade. The physical process that is behind giant magnetoresistance is spin-dependent scattering of conduction electrons in ferromagnetic materials.

2.1 Introduction

According to the two-current model [12], one spin component of the current is less strongly scattered than the other component, if the two ferromagnetic layers are magnetized parallel. In an antiparallel alignment, however, both spin components are equally strongly scattered. This results in lower resistance for the parallel than for the antiparallel alignment. The origin of spin-dependent scattering in transition metals can be understood by considering the fact that the charge carriers, the sp electrons, are predominantly scattered into unoccupied d states [13]. This leads to spin-dependent scattering in ferromagnetic transition metals because there are more empty minority-spin d states available for scattering than empty majority-spin d states.

2.1.1 Spin-Dependent Electron Absorption

Experimental evidence for spin-dependent scattering of hot electrons in ferromagnets comes from overlayer experiments with spin-polarized photoemission (see, for example, [14]). Unpolarized electrons from a nonmagnetic substrate are found to become polarized after traversing a thin ferromagnetic film. Remarkably, an empirical rule for inelastic scattering of electrons in transition metals has been found by a compilation of many such overlayer experiments

on a number of materials [15]. This rule says that absorption is divided into a term that accounts for scattering into unoccupied states other than d states and a term that is proportional to the number of holes available to one spin state in d orbitals. The most interesting consequence of this proportionality is that absorption becomes spin-dependent for ferromagnetic transition metals because the number of holes is different in the two spin directions. Hence, majority-spin electrons traveling across a ferromagnetic material are more easily transmitted than minority-spin electrons.

A different approach from the overlayer experiments to investigating spin-dependent electron scattering is experiments where the transmission of a spin-polarized free electron beam across metal foils is studied [16,17]. The results of this type of experiment are presented in this chapter.

2.1.2 Spin Motion

Numerous studies have been done previously on the interaction of spin-polarized electrons with ferromagnets, but this "spin motion" experiment is distinguished by the fact that the spin polarization vector $\boldsymbol{P}_0$ of the incident electrons is at an angle of $\vartheta = 90°$ to the magnetization vector $\boldsymbol{M}$; in all earlier experiments, $\boldsymbol{P}_0$ was either parallel or antiparallel to $\boldsymbol{M}$. Only with this non-linear initial configuration, can the motion of the spin polarization vector be observed.

To analyze this particular spin configuration, we consider the spin part of the wave function of a single electron whose spin is perpendicular to $\boldsymbol{M}$. In this case, it is a coherent superposition of a majority-spin (parallel to $\boldsymbol{M}$) and a minority-spin (antiparallel to $\boldsymbol{M}$) wave function. Because these spin wave functions are represented by a (1,0), respectively (0,1) spinor, $\psi_0 \sim [(1,0)+(0,1)]\mathrm{e}^{i\varphi}$. The two partial waves have an arbitrary but identical phase φ prior to the interaction with the ferromagnet. If one now takes into account that the interaction with the ferromagnet is spin-selective, the transmitted, respectively, reflected intensity of the majority spins I^+ will be different from that of the minority spins I^-. This defines the spin asymmetry $A = (I^+ - I^-)/(I^+ + I^-)$ for a pure spin state ($P_0 = 1$). Furthermore, majority-spin and minority-spin waves may have different phase velocities that lead to a difference ϵ in phase between the two partial waves after a time t of interaction: $\epsilon = \Delta E_{\mathrm{ex}} \cdot t/\hbar$. $\Delta E_{\mathrm{ex}} = E^- - E^+$ is the difference between the energy of the minority spins E^- and the energy of the majority spins E^+, the so-called exchange energy.

In transmission, time t is – if we neglect quantum resonance effects – simply given by $t = d/v$ where d is the thickness of the ferromagnetic film and v is the group velocity of the electrons. We can estimate ϵ in transmission by assuming free electron behavior, which is reasonable for electrons in the energy range of interest. Then, the group velocity is simply $v = \sqrt{2E/m}$, where m is the free electron mass and E is the energy of the primary electron beam measured with respect to the inner potential of the ferromagnet.

Therefore one obtains, $\epsilon = \sqrt{\frac{m}{2\hbar^2}}\frac{\Delta E_{\mathrm{ex}}}{\sqrt{E}} \cdot d$. Assuming an exchange splitting of several tenths eV – a reasonable value in the investigated energy regime, where we are dealing with sp bands – one obtains a specific precession angle $\tilde{\epsilon} = \epsilon/d$ of the order of 10° per nanometer of ferromagnetic film thickness.

In reflection, interaction time t is determined by the length of the pathway within the material; hence, t is governed by the absorptive properties of the ferromagnet. Therefore, the precession angle ϵ in reflection is determined by both the exchange interaction and the spin-dependent absorption. Furthermore, there may also be a jump in phase upon reflection of the waves. If this jump is of different magnitude for majority-spin and minority-spin waves or if it occurs at different energies, there will be an additional contribution to ϵ [18].

The spin part of the wave function of the electron after interaction with the ferromagnet is then $\psi \sim [\sqrt{1+A}(1,0)\mathrm{e}^{-\mathrm{i}\epsilon/2} + \sqrt{1-A}(0,1)\mathrm{e}^{\mathrm{i}\epsilon/2}]\mathrm{e}^{\mathrm{i}\varphi}$. Now, taking into account the incomplete spin polarization P_0 of the incident electron beam, the expectation values of the Pauli matrices σ_x, σ_y, and σ_z yield the spin polarization of the transmitted, respectively, reflected beam: $\boldsymbol{P} = (P_0\sqrt{1-A^2}\cos\epsilon, P_0\sqrt{1-A^2}\sin\epsilon, A)$. This corresponds to a precession of the spin polarization vector about $\boldsymbol{M}$ by an angle of ϵ and a change in the angle ϑ (Fig. 1). The angle ϑ is given by $\vartheta = \arctan(P_0\sqrt{1-A^2}/A)$. Therefore, ϑ smaller than 90° means that minority spins are absorbed more efficiently in a ferromagnet compared to majority spins.

The precession of the spin-polarization vector about $\boldsymbol{M}$ is reminiscent of the rotation of the plane of polarization in magneto-optics that is observed when a polarized light beam interacts with a ferromagnet. In fact, there is a complete analogy between electrons and light if for photons, the three-dimensional Poincaré representation (in abstract polarization space) is

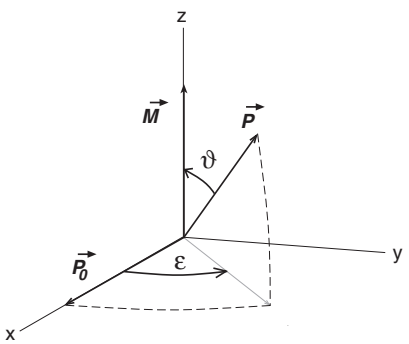

Fig. 1. Schematic drawing of the two types of movement of a spin-polarization vector. The angle ϑ changes its value due to the difference in the amplitudes of the majority-spin and the minority-spin wave functions. The difference in the phase factors between the two spin functions, on the other hand, causes the spin-polarization vector to precess about $\boldsymbol{M}$ by an angle of ϵ

considered. Poincaré suggested mapping the settings of a complete polarization analyzer for light onto a sphere. The origin of this correspondence is the well-known fact that the mathematical descriptions of a polarized light beam and a nonrelativistic electron beam, as in our case, are analogous [19]. However, the strength of this effect with electrons is about two orders of magnitude larger. Precession of the order of 10°/nm is expected for electrons in transmission geometry (see above), but values of only 0.1°/nm are found for photons in the Faraday configuration [20]. This difference in the strength of "magneto-optic" phenomena arises because the electron spin couples directly to magnetization, whereas coupling of photons to magnetization must be mediated by spin – orbit interaction.

2.2 Experiment

The experimental setup is sketched in Fig. 2. A spin-polarized electron source based on a GaAs photocathode produces a spin-polarized free electron beam by optical pumping with circularly polarized light. By switching from right to left circularly polarized light for excitation of the source, we can invert the polarization vector $\boldsymbol{P_0}$. It is also possible to produce an unpolarized electron beam by using linearly polarized light. By applying a combination of electric and magnetic fields to the electron beam, $\boldsymbol{P_0}$ can be rotated into any desired direction in space. In transmission experiments (Fig. 2a,b), the electron beam impinges normally onto a ferromagnetic film of varying thickness sandwiched between Au layers, which serve both as supporting and protective layers. The incident spin-polarization vector $\boldsymbol{P_0}$ is either parallel/antiparallel to $\boldsymbol{M}$ in the absorption experiment (Fig. 2a) or perpendicular to $\boldsymbol{M}$ in the "spin motion" experiment (Fig. 2b). In the reflection experiment (Fig. 2c), the spin-polarized electron beam impinges on a ferromagnetic Co film at an angle of 45° with respect to the surface normal. Ferromagnetic films are remanently magnetized in the easy direction of magnetization by applying a magnetic field pulse. The transmitted, respectively, specularly reflected, electrons are energy analyzed by a retarding grid analyzer that has an energy resolution of 0.5 eV. The electrons are either detected in a Faraday cup in the absorption experiment or subsequently accelerated to an energy of 100 keV to measure the transverse components of the spin-polarization vector via Mott scattering in the "spin motion" experiment. To distinguish precession from rotation, the direction in space as well as the relative alignment of $\boldsymbol{P}_0$ and $\boldsymbol{M}$ are interchanged. On reversing $\boldsymbol{P}_0$, only ϵ changes sign, whereas on reversing $\boldsymbol{M}$, the sense of both precession and rotation change sign. Hence, it is possible to obtain the contribution of each motion separately. The technique of changing both the absolute direction of $\boldsymbol{P}_0$ and $\boldsymbol{M}$ as well as their relative orientation also eliminates the effects of spin – orbit interaction.

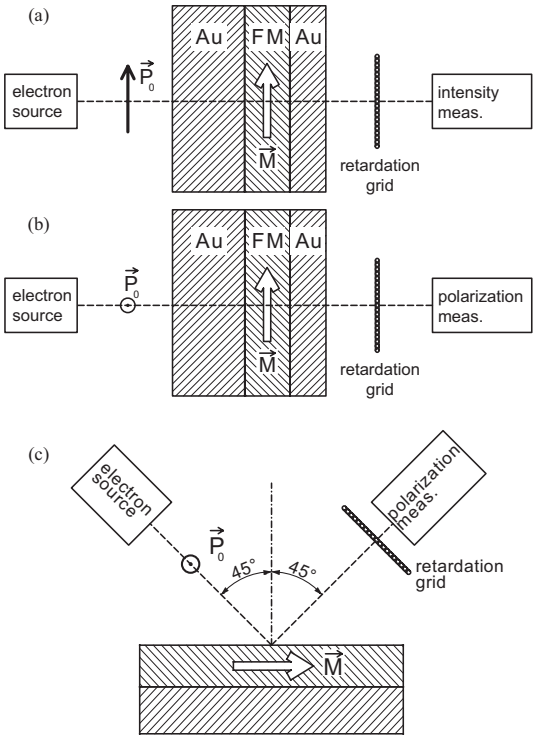

Fig. 2. The principle of the experiment. It consists of a spin-polarized electron source of the GaAs type, a ferromagnetic film that is magnetized remanently in-plane, a retardation grid for the energy analysis, and a detection system. In the latter, the intensity and/or the degree of spin polarization perpendicular to the axis of the outgoing electron beam is measured. (**a**) Measurement of the spin-dependent absorption with $\boldsymbol{P}_0$ parallel or antiparallel to $\boldsymbol{M}$. (**b**) Measurement of the spin motion in transmission geometry with $\boldsymbol{P}_0$ perpendicular to $\boldsymbol{M}$. (**c**) Measurement of the spin motion in reflection geometry with $\boldsymbol{P}_0$ perpendicular to $\boldsymbol{M}$

2.3 Samples

2.3.1 For the Transmission Experiment

Because electron–electron scattering produces inelastic mean free paths of the order of 1 nm or even less in transition metals [15], the film has to be extremly thin to observe the emerging electron beam. In fact, the experiment cannot be done with a self-supported film of only a transition metal. Rather, one has to use the fact that electron scattering is reduced in noble metals like Au. A Au film about 20 nm thick, which is used as a substrate for the ferromagnetic transition metal, attenuates a low-energy electron beam by only 10^4–10^5 making it still possible to measure transmitted electron intensity.

Finally, the polycrystalline ferromagnetic Fe, Co, or Ni film is capped with a protecting Au layer 2 nm thick.

The trilayers are made in a separate UHV chamber on a substrate consisting of a film of nitrocellulose supported by a Si wafer with a number of 0.5-mm wide apertures. All metals are deposited by electron beam bombardment. The thickness is measured by a quartz microbalance, which is calibrated by profilometry. For magnetic characterization, the in-situ longitudinal magneto-optic Kerr effect is used. Figure 3 shows the Kerr intensity I_K, defined as the difference between the light intensity in positive and negative saturation fields, as a function of the ferromagnetic film thickness of Fe, Co, and Ni (before Au capping). By extrapolating the variation in I_K versus film thickness linearly, one obtains the intercept at the horizontal thickness axis. This intercept is the thickness of the magnetic dead layer d_0 (at room temperature). d_0 is 0.3 and 0.2 nm for Fe and Co, respectively, but Ni has a much thicker magnetic dead layer of ~ 2 nm. Note that for Ni thicknesses below 2 nm, no Kerr signal is observed in polar Kerr geometry as well, so that out-of-plane magnetization can be excluded. The most likely reason for this failure to observe magnetism in thin layers is the diffusion of Au atoms into the ferromagnetic layer.

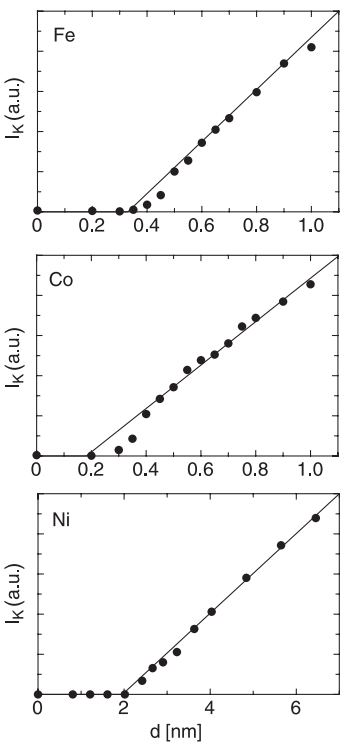

Fig. 3. The longitudinal magneto-optic Kerr intensity I_K as a function of the ferromagnetic film thickness of a ferromagnet/Au double layer (*top*: Fe, *middle*: Co; *bottom*: Ni). The intercepts of the straight lines with the thickness axis determine the thicknesses d_0 of the magnetic dead layers

In all cases, uniaxial magnetic in-plane anisotropy occurs, which may be attributed to the nonnormal incidence of the growth beam during deposition. By measuring along the easy magnetization axis, the hysteresis loops exhibit full magnetic remanence. Thus, we are sure that magnetization will not decay into domains after the application of a magnetic field pulse. This is very important for our experiments because any constant applied magnetic field would deflect the electron beam. After the magnetic tests are completed, the whole sample is opened to air, and the nitrocellulose on the apertures is removed by putting the sample into acetone. The sample is then introduced through a load-lock system into the chamber with the spin-polarized electron source. There, the sample is sputtered to thin the supporting Au layer until low-energy electrons are transmitted at an attenuation of not more than 10^6. The Kerr hysteresis loops taken later show no difference from the loops obtained just after deposition of complete trilayers.

The preparation of pinhole-free self-supported layers is crucially important in transmission experiments. The easiest method for checking for the existence of pinholes is to investigate the energy dependence of the elastic intensity. For primary electron energies around 30 eV, the inelastic mean free path is smallest [21] and too short for an elastic signal to be observed at the film thicknesses investigated. Thus, any pinhole that leads to an elastic signal larger than our detection limit can be excluded by measuring at primary energies around 30 eV. If there is the tiniest pinhole, the main part of the elastic signal observed at the back side of the trilayer is caused by electrons that have passed through the pinhole. We suspect that this is the reason why in experiments by *Drouhin* et al. [22], an almost constant attenuation factor of about 10^5 was found across the same energy range. The steep increase in attenuation with increasing primary energy in our data (Fig. 4) is in reasonable agreement with the energy dependence of the electron mean free path in Au [23].

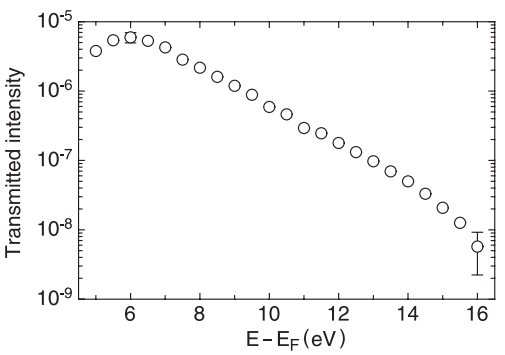

Fig. 4. The attenuation of elastic electrons after penetration of the trilayer versus the primary energy above the Fermi energy E_F. Note the logarithmic plot

2.3.2 For the Reflection Experiment

The samples investigated here are Co films grown on two types of substrates, a (111)-textured polycrystalline Au film on glass and a Cu(001) single crystal. The metal films are deposited by electron beam bombardment, and their thickness is measured by a quartz microbalance. The details of film growth are described in [24] and [25], respectively. The first type of substrate generates a polycrystalline Co film, and the second type of film grown on Cu(001) is single crystalline fcc-Co. The experiments are done in UHV with an atomically clean surface. Magnetic characterization is again achieved by using the magneto-optic Kerr effect. In polycrystalline Co/Au/glass films, the easy direction of magnetization is induced by oblique incidence of the atom beam during deposition. In fcc-Co, the easy direction is in one of the (110) directions [25]. Of importance to the present experiment is again the observation that both types of films exhibit full magnetic remanence, i.e., they can be investigated while in a single-domain state without applying an external magnetic field.

2.4 Results

2.4.1 Spin-Dependent Electron Absorption (Mostly Co)

Transmission Experiment. Figure 5 shows data observed with an incident electron beam of about 7 eV energy and $\boldsymbol{P_0}$ either parallel or antiparallel to the magnetization direction of a polycrystalline Co film 4 nm thick. One observes two different energy distribution curves of the emerging electron beam. I^+ is valid for $\boldsymbol{P_0}$ parallel and I^- for $\boldsymbol{P_0}$ antiparallel to $\boldsymbol{M}$. The elastic part of the beam displays huge spin asymmetry A for a pure spin state ($P_0 = 1$). On the other hand, the inelastic part of the electron spectrum exhibits lower A. This is mainly due to the occurrence of secondary electrons. Although secondary electrons that are generated in a ferromagnet are spin-polarized, they have lost the memory of the primary spin polarization and thus reduce the spin asymmetry. In the following, we focus on the elastic part of the spectrum.

Now, we consider electron absorption in the Co film of thickness d for each spin direction separately. With incident current I_0, the transmitted elastic current is $I = I_0 \mathrm{e}^{-\sigma d}$. The absorption coefficient σ depends on the angle between $\boldsymbol{P_0}$ and $\boldsymbol{M}$; the largest value σ_- occurs for antiparallel alignment, and the smallest σ_+ for the parallel alignment of $\boldsymbol{P_0}$ and $\boldsymbol{M}$. With $\Delta\sigma = \sigma_- - \sigma_+$, $A = (\mathrm{e}^{\Delta\sigma d} - 1)/(\mathrm{e}^{\Delta\sigma d} + 1)$, and $\Delta\sigma = (1/d)\ln[(1 + A)/(1 - A)]$.

Figure 6 shows $\Delta\sigma$ as a function of the primary energy obtained with samples of different Co thickness. To interpret this further, we assume that all spin-dependent scattering is scattering on the d shell, and that the strength of the scattering is proportional to the number of holes in that shell. The number of holes in the d shell is not known a priori for atoms in a metal.

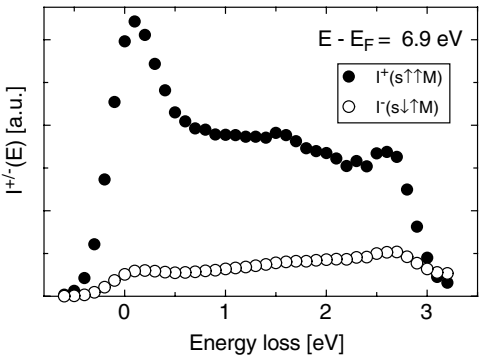

Fig. 5. The intensity distribution curves $I^+(E)$ and $I^-(E)$ are shown for a polycrystalline Co film 4 nm thick. $I^+(E)$ is valid for spin parallel to the magnetization $\boldsymbol{M}$, and $I^-(E)$ for spin antiparallel to $\boldsymbol{M}$. The energy of the primary electrons is fixed at 6.9 eV above E_F. The data are normalized to $P_0 = 1$

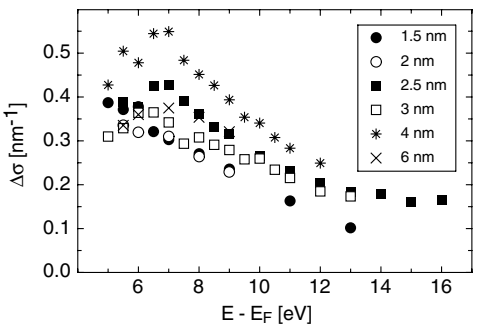

Fig. 6. Difference in the absorption coefficient $\Delta\sigma$ for majority- and minority-spin electrons versus electron energy for a number of samples with different Co thicknesses

However, with ferromagnetic metals, one knows the spin part of the saturation magnetization, which is mainly given by the difference in the occupancy of the d shell between majority- and minority-spin electrons, known as the number of Bohr magnetons, n_B, per atom. Because the present electron energies are several eV above E_F, all of the d holes are available for scattering. This yields $\Delta\sigma = n_\mathrm{B}\sigma_\mathrm{d}$ where σ_d is the absorption coefficient for one unoccupied state in the 3 d shell in Co. This approach is well supported by a number of quite different experiments [26]. Although there is significant scatter among the different samples in Fig. 6, all exhibit a clear decrease in $\Delta\sigma$ with increasing primary electron energy. This shows that the matrix element for scattering into the Co 3 d shell decreases with increasing energy. This is reasonable because the probability of a single relaxation step into the d band becomes smaller with increasing energy distance between the primary electron and the Fermi energy, around which the d band is located.

One must be aware that inelastic as well as elastic scattering on the d shell may contribute to $\Delta\sigma$. *Gokhale* and *Mills* [27] have shown in the example

of a single crystalline Fe film that the effects of elastic exchange scattering may lead to sizable contributions to spin-dependent transmission. However, we can easily test how important elastic exchange scattering actually is in our experiments. This test consists of two parts. First, an unpolarized electron beam passes through the ferromagnet. This produces a spin polarization P that consists of two contributions, $P = P' + \Delta P$. P' is the transport polarization generated by spin-selective scattering into the holes of the d band [15], and ΔP is the additional spin polarization generated by elastic exchange scattering. Second, a polarized electron beam with initial polarization P_0 passes through the ferromagnet. The spin asymmetry A is given by $A = A' - \Delta A$, where A' is the asymmetry due to inelastic spin-selective absorption [17] and ΔA is the reduction of this asymmetry because some electrons have flipped their spin in elastic exchange collisions and thus avoided spin-dependent absorption. We find within the experimental uncertainty that $P = A$ for a 5-nm thick Fe film (see Fig. 7). Because a polarizing spin filter must be equal to an analyzing spin filter in the absence of spin-productive scattering such as exchange scattering, i.e., $P' = A'$, both ΔP and ΔA must be zero. Thus, elastic exchange scattering is not important in this experiment. We believe therefore that the main contribution to scattering on the d shell is predominantly inelastic.

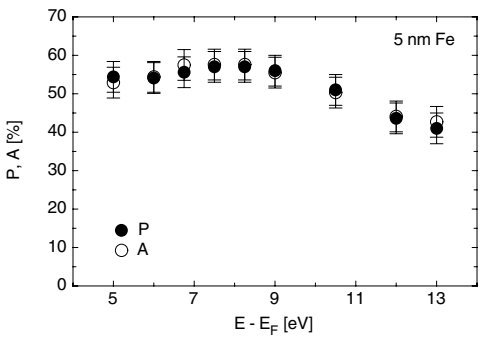

Fig. 7. Both the spin asymmetry A (measured with a polarized incident electron beam) and the degree of spin polarization P (measured with an unpolarized incident electron beam) of elastic electrons for a 5-nm thick Fe film are shown as functions of primary electron energy

Time-Resolved Experiment. The absorption of electrons due to inelastic scattering must correspond to a finite relaxation time of the electrons. It can be determined directly in pump-probe experiments employing ultrafast laser pulses. The absorption of the pump photon brings an electron to the intermediate energy level E^* above the Fermi energy E_F. If the probe photon is absorbed while the electron is still at E^*, it can escape into vacuum. By

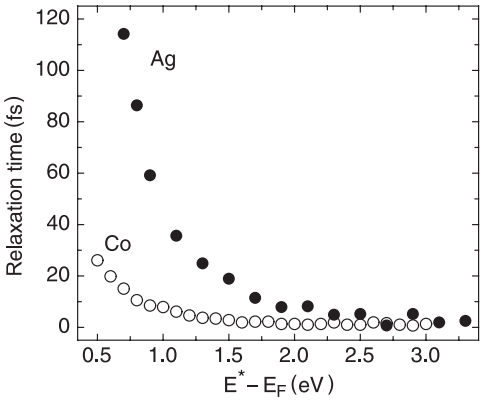

Fig. 8. The spin-integrated relaxation time of thick films of Co(001) and Ag(111) as functions of the intermediate state energy E^* above E_F. The photon energy is 3 eV and 3.3 eV, respectively. *Closed symbols*: Ag(111); *open symbols*: Co(001)

setting the energy analyzer to transmit electrons at a specific kinetic energy, E^* can be varied. Now, if the delay between the pump- and the probe-photon pulse is increased, one sees a decrease in the detected electron intensity reflecting the finite relaxation time in the intermediate state E^*. Figure 8 shows results with the noble metal Ag, in which the d band is fully occupied, and with Co [28]. One sees that the relaxation time of hot electrons is much smaller in Co than that in Ag, which is due to the fact that the partially unoccupied d band of Co offers a lot of open scattering channels. It is also seen that the spin-integrated relaxation time increases as one approaches E_F in both metals. This behavior is explained by a reduction in the phase space for electron–electron scattering, which is the dominant scattering contribution in the energy regime investigated. Because absorption is spin-dependent within a ferromagnet, we also expect that the relaxation time must depend on the spin state as well. This is observed by measuring the spin state of the electrons emitted in the pump-probe experiment [28]. Figure 9 shows spin-dependent relaxation times as a function of intermediate state energy E^* for a Co(001) surface [29]. Understanding the detailed behavior of spin-dependent relaxation time is complicated and requires considering the actual electronic band structure of Co(001). Moreover, it must be emphasized that the pump-probe process also has several weaknesses in interpretation. The number of electrons at E^* that can escape into vacuum is reduced also by diffusion of the electrons into the bulk. On the other hand, this number is increased by electrons relaxing from higher states into E^*. The holes in the d band left behind after excitation of the photoelectron will produce Auger electrons, complicating further a detailed interpretation. Yet, the pump-probe experiment is clearly consistent with the spin-dependent electron–electron scattering model.

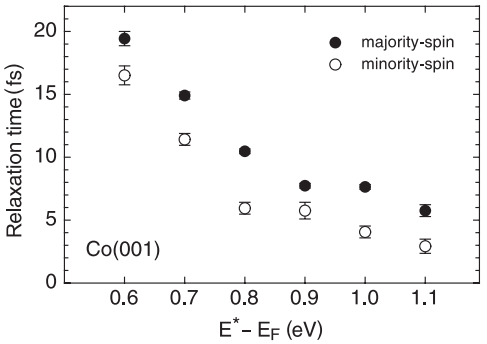

Fig. 9. Spin-resolved relaxation time of a 10 nm thick Co(001) film versus intermediate state energy E^* above E_F. *Closed symbols*: majority-spin electrons; *open symbols*: minority-spin electrons. The photon energy is 3 eV

2.4.2 Spin Motion (Fe, Co, and Ni)

Transmission Experiment. The $\vartheta(d)$ values (normalized to $P_0 = 1$) are shown in Fig. 10. In all cases, ϑ decreases with increasing film thickness, i.e., the spin-polarization vector turns more and more in the direction of $\boldsymbol{M}$ with increasing thickness [10]. As shown in Sect. 2.1.2, angle ϑ is solely determined by spin asymmetry A due to spin filtering. Thus, it is readily seen that the strength of spin filtering in Fe and Co is similar, whereas spin filtering is much less effective in Ni. The spin asymmetry $A(d)$, which enters the expression for $\vartheta(d)$, can be rewritten as $A(d) = \tanh[\Delta\sigma(d-d_0)/2]$ if we take into account the existence of magnetic dead layers of thickness d_0. The curves through the data points represent fits based on this expression. Using both the fitted $\Delta\sigma$ and the known values of the spin-integrated absorption coefficient σ [15], the ratio σ_-/σ_+ of the spin-dependent absorption coefficients can be determined for each ferromagnet: 1.5 for Fe, 1.67 for Co, and 1.13 for Ni.

The dependences of precession angle ϵ on film thickness d for Fe, Co, and Ni, shown in Fig. 11, are valid for elastic electrons at 7 eV above the Fermi energy E_F [10]. The data point at $d = 0$ was taken with the Au substrate alone, showing that $\boldsymbol{P}$ does not precess in Au, as expected. A linear fit describes the observations in all three ferromagnets, indicating that the precession is a bulk property of the ferromagnets. The slope is the specific precession angle $\tilde{\epsilon} = 33°/\text{nm}, 19°/\text{nm}$, and $7°/\text{nm}$ for Fe, Co, and Ni, respectively. As in the fits to the $\vartheta(d)$ data, nonzero d_0 values have to be taken into account [30]. We do not discuss the reasons for the occurrence of d_0 in more depth because we are focusing in this paragraph on the bulk effects of the ferromagnet extracted with the specific precession angle $\tilde{\epsilon}$.

The energy dependence of ϵ for all three ferromagnets is shown in Fig. 12. For Co and Ni, the variation of ϵ in the low-energy regime is weak and can be explained mainly by the change in group velocity v in $\epsilon = \Delta E_{ex}/v$. Thus the exchange energy ΔE_{ex} is quite constant in the low-energy range. On the other

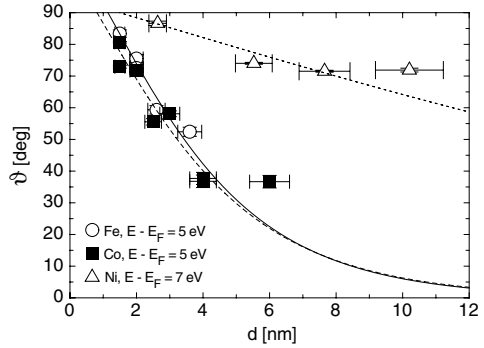

Fig. 10. The angle ϑ enclosed by $\boldsymbol{P}$ and $\boldsymbol{M}$ as a function of the ferromagnetic film thickness for Fe, Co, and Ni, measured with elastic electrons of energy $(E - E_\mathrm{F}) = 5$ and 7 eV. Note that the values of the angle ϑ are normalized to $P_0 = 1$ (pure spin state). The curves through the data points represent fits based on the expression given in the text (Fe: *continous line*, Co: *dashed line*, Ni: *dotted line*)

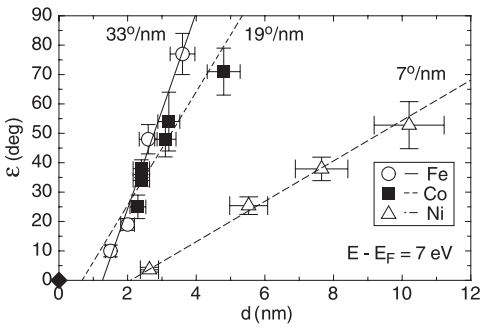

Fig. 11. The spin precession angle ϵ as a function of the ferromagnetic film thickness for Fe, Co, and Ni, measured with elastic electrons of energy $(E - E_\mathrm{F}) = 7$ eV. The point at zero thickness was measured with a pure Au film 20 nm thick. The *straight lines* through the data points represent linear fits

hand, Fe exhibits much stronger energy dependence and a maximum at 9 eV above E_F. One is tempted to attribute this maximum in ϵ to a maximum in exchange energy. However, we have reasons to believe that this nonmonotonic behavior is rather the result of varying group velocity around 9 eV above E_F. In fact, band structure calculations of Fe [31] reveal a flattening of bands and thus a decrease in group velocity around 9 eV above E_F.

We also investigated the spin precession of Fe and Co at much higher energies (see insets in Fig. 12), where the larger inelastic mean free path allows transmission experiments again. At intermediate energies, the transmitted current was too small to be detected because of the inelastic mean free path minimum in this energy range [21]. In both cases, small but significant precession angles of a few degrees are found. One might ask if these nonvanishing

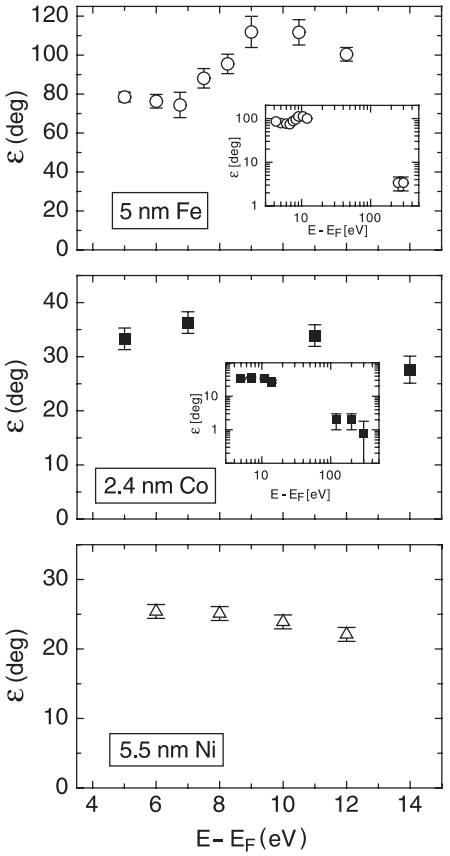

Fig. 12. The spin precession angle ϵ as a function of electron energy for Fe (*top*), Co (*middle*), and Ni (*bottom*). The *insets show* ϵ across a wider energy range. Note the double logarithmic plot

values of ϵ are actually due to nonvanishing exchange energy. Can the stray field of the ferromagnetic sample cause such small precession angles? It can. However, the direction of the stray field outside the ferromagnet is opposite to the magnetization direction and should therefore result in a negative value of ϵ, whereas positive values are found in the experiment.

From the data, we readily recognize that the increase in group velocity (roughly by a factor of 3) from the low-energy to the high-energy regime, can only partly explain the observed reduction in ϵ. Thus, there must also be a strong decrease in exchange energy with increasing energy. This is in accordance with calculations that show a clear decrease in ΔE_{ex} with increasing energy [32]. The higher the energy, the weaker the exchange interaction between the quasi-free injected electrons and the d electrons below the Fermi level.

Reflection Experiment. Figure 13 shows the experimental results for ϵ and ϑ obtained with polycrystalline and single crystalline Co films and with

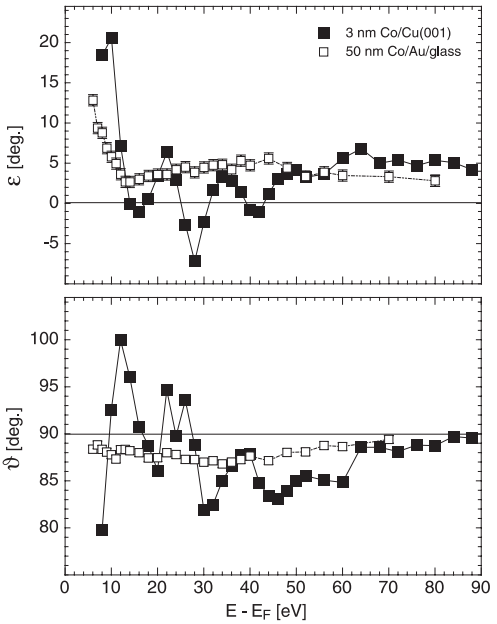

Fig. 13. The angle ϵ of precession and the angle ϑ of rotation of $\boldsymbol{P}$ with single crystalline (*closed symbols*) and polycrystalline Co (*open symbols*) versus the energy of electrons above the Fermi energy. The lines are guides to the eye

elastic reflection of electrons of energy 5–90 eV above the Fermi energy. With the polycrystalline film, ϵ is always positive, and ϑ is always reduced from the initial value of 90°. Therefore, the precession about $\boldsymbol{M}$ always has the sense of a right-handed screw independent of the energy of the electrons, and the sense of the rotation indicates that $\boldsymbol{P}$ and $\boldsymbol{M}$ tend toward parallel alignment. The same behavior of $\boldsymbol{P}$ has also been observed with electrons injected into the bulk of polycrystalline Ni, Fe, and Co (see the preceeding paragraph) [10]. This sense of the precession of $\boldsymbol{P}$ is explained by the exchange field to which an electron is subjected as soon as it interacts with ferromagnet, whereas the rotation into $\boldsymbol{M}$ has been explained by preferential inelastic scattering of minority spins into the holes of the 3 d shell [17]. However, Fig. 13 shows that with single crystalline Co, both precession and rotation show strong changes, in particular of the sign, as the energy is varied. Therefore, different additional mechanisms must be operative in a single crystal.

We propose that the band gaps in crystalline material cause this special behavior of crystalline ferromagnetic surfaces. It is well known that spin-dependent band gaps dominate the reflection of electrons from single crystalline surfaces; in fact, this is used to image magnetization [33] and to detect electron spin polarization efficiently [34]. As the energy is varied across a band gap, first the majority spins will be preferentially reflected in the middle of the majority gap. Subsequently, the minority spins will be preferentially reflected in the middle of the minority gap which lies higher in energy by the exchange splitting ΔE_{ex}. Thus, the existence of exchange splitting causes

a change in the spin asymmetry A and thus a change in sign of $\cos\vartheta$. There is also an increasing phase shift of the wave function on changing the energy from the top of the lower band to the bottom of the higher band [35]. This phase shift occurs at different energies for up and down partial waves – again because of the nonvanishing exchange splitting – and hence leads to a contribution to ϵ. The band gaps should therefore produce changes in the sign of $\cos\vartheta$ accompanied by changes in the relative phase shift ϵ.

Figure 13 shows that structures in ϵ and ϑ occur at $E - E_\mathrm{F} = 16\,\mathrm{eV}$, 28 eV, and 41 eV. To establish whether there are absolute or relative band gaps at these electron energies with the present experimental geometry, band structure calculations were done [36]. Band structures in high symmetry $\boldsymbol{k}$-directions of the Brillouin zone are not sufficient. Instead, for each energy, an independent calculation has to be done. $a = 0.355\,\mathrm{nm}$ for the lattice constant in the bulk and at the surface of fcc-Co has been assumed. The inset in Fig. 14 shows the resulting band structure along the crystal wave vectors $(2\pi/a)(0.425, 0.425, 0) \leq \boldsymbol{k} \leq (2\pi/a)(0.425, 0.425, 1)$ and $(2\pi/a)(0.2, 0.2, 0) \leq \boldsymbol{k} \leq (2\pi/a)(0.2, 0.2, 1)$. These two $\boldsymbol{k}$-lines have to be considered if we want to know the conditions encountered by the electrons of 16 and 28 eV, respectively. The calculations reveal band gaps around these energies. The agreement between the energies of the structures observed in ϵ and ϑ and the location of the band gaps is not perfect but is satisfactory, considering the uncertainties in the theory as well as in the experiment. For the third structure at 41 eV, we have not been able to find correlations with the band structure because of the multitude of the bands involved at this energy.

Figure 14 also shows a remarkable additional result of this experiment. The derivative $\mathrm{d}\epsilon/\mathrm{d}E$ traces closely the energy dependence of ϑ. Elementary optical dispersion theory connects the reflection, absorption, and the index of refraction n. $1/n$ is proportional to the phase velocity in the medium which changes abruptly depending on the width and magnitude of the reflection peak. With spin-polarized electrons, $\mathrm{d}\epsilon/\mathrm{d}E$ highlights the jumps in the relative phase shift of spin-up against spin-down partial waves, and ϑ signals the spin-dependent reflection. Figure 14 thus suggests that there is a physical analogy between magneto-optics and spin-polarized electron scattering that goes beyond the mathematical equivalence in the description of polarization phenomena. In fact, the present experiment is precisely analogous to the longitudinal magneto-optic Kerr effect. In both optics and spin-polarized electron scattering, the matrix F that connects the incident wave ψ_0 with the reflected wave $\psi = F\psi_0$ contains the material constants A and ϵ, and the off-diagonal elements that mix the two polarizations or spin channels, respectively, remain zero. Of course, both A and ϵ are much larger with electrons due to the direct coupling of spin to magnetization. This makes spin-polarized electrons the preferred "magneto-optic" tool in nanomagnetism.

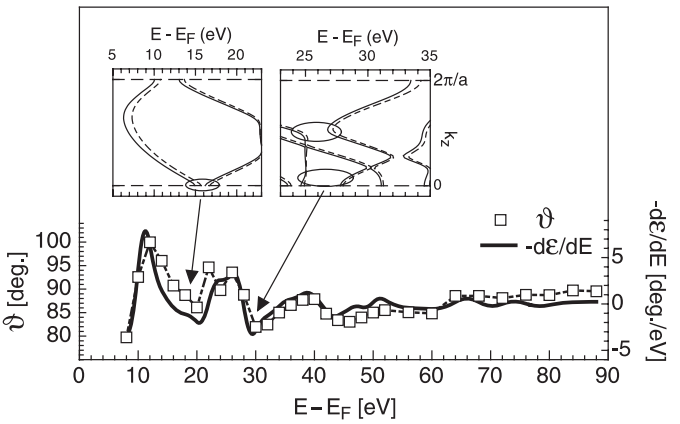

Fig. 14. The derivative $\mathrm{d}\epsilon/\mathrm{d}E$ of the precession angle versus energy for single crystalline Co. $\vartheta(E)$ is replotted from Fig. 13. The lines are guides to the eye. The inset shows the result of self-consistent band structure calculations along the $\boldsymbol{k}$-lines relevant in the experiment (*solid lines*: majority-spin bands, *dashed lines*: minority-spin bands). *Left*: $k_x = k_y = 0.425 \cdot (2\pi/a)$. *Right*: $k_x = k_y = 0.2 \cdot (2\pi/a)$. In both cases, k_z varies between 0 and $2\pi/a$

Figure 15 shows the variation of the precession angle ϵ with the thickness of single crystalline fcc-Co film on the Cu(001) substrate. Because Cu will not produce any precession, one expects that ϵ grows from zero to its final saturation value when the thickness of Co is of the order of the penetration depth of the electrons and/or when the spin-polarized ferromagnetic band structure of Co has reached a stable final configuration. At 9 eV energy, saturation is reached, yielding an inelastic mean free path λ of about 1 nm [37]; at 28 eV, a linear decrease of ϵ occurs up to 20 nm thickness followed by a slower increase at still greater thickness. The first observation is roughly consistent with the fact that the inelastic mean free path of low-energy electrons found in Co was 0.8 nm in a number of independent experiments [15]. The second observation signals that the band structure may still not be stable upon film growth even to sizable thicknesses. It is known that the strain induced by the misfit between the Co overlayer and the Cu substrate relaxes from 2 nm thickness onward, but even at 7 nm, the lattice parameter of a Co film is still changing in both the interior and at the surface [25]. This may explain the decrease in ϵ in this thickness range, assuming extraordinary sensitivity of the hybridization gap at 28 eV to the crystal structure. This sensitivity contrasts with the stability of ϵ at the first band gap at 16 eV. It is also known that the transformation of fcc-Co into hcp-Co occurs from 20 nm thickness onward [38], which correlates with the observed turning point of $\epsilon(28\,\mathrm{eV})$ at this thickness. Hence, the increase of $\epsilon(28\,\mathrm{eV})$ from 20 nm onward may be explained by crystal transformation. This demonstrates yet another application

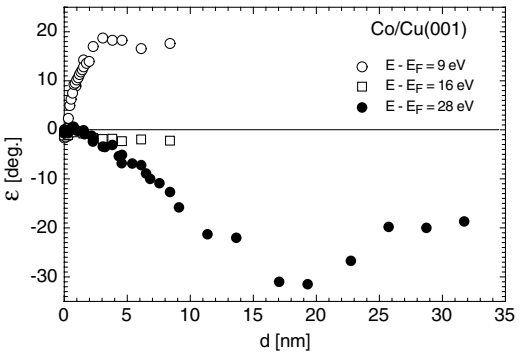

Fig. 15. The precession angle ϵ versus thickness of the single crystalline fcc-Co layer at three selected electron energies

of the reflection experiment to material characterization which is analogous to ellipsometry on metals with polarized light.

3 Magnetic Phenomena Generated by an Exchange Field

The precession of the electron spin polarization vector about $\boldsymbol{M}$ can be viewed as the Larmor precession of the electron spin about an effective magnetic field. Such a point of view is justified by the fact that the exchange interaction between the spins in a ferromagnet acts as if there were a magnetic field acting on each spin, the exchange field $\boldsymbol{B}_{\mathrm{ex}}$. We note, however, that the exchange field is by no means equivalent to a regular magnetic field because it produces no Lorentz force on the electrons and its changes with time do not induce eddy currents.

3.1 The Torque Acting on Magnetization by Hot Spins

The exchange field is a function of both electron energy and linear momentum, and it is an axial field parallel to $\boldsymbol{M}$. $\boldsymbol{B}_{\mathrm{ex}}$ exercises a torque $\boldsymbol{\tau}_{\mathrm{e}}$ on any electron introduced into the ferromagnet. This torque is given by $\boldsymbol{\tau}_{\mathrm{e}} = \boldsymbol{\mu}_{\mathrm{e}} \times \boldsymbol{B}_{\mathrm{ex}} = -(g\mu_{\mathrm{B}}/\hbar)\boldsymbol{s} \times \boldsymbol{B}_{\mathrm{ex}}$ where $\boldsymbol{\mu}_{\mathrm{e}}$ is the magnetic moment of the electron, g is the gyromagnetic factor, which is assumed in the following to be exactly two as reasonable for nonrelativistic electrons, μ_{B} the Bohr magneton, and $\boldsymbol{s}$ the injected electron spin. $\boldsymbol{\tau}_{\mathrm{e}}$ leads to precession of $\boldsymbol{s}$ about $\boldsymbol{B}_{\mathrm{ex}}$ with a frequency $\omega_{\mathrm{e}} = (e/m)B_{\mathrm{ex}}$ (e: elementary charge).

Once an electron has crossed the surface barrier and is inside the ferromagnet, we have a closed system with no external forces. Hence, the total angular momentum $\boldsymbol{L}$ consisting of the angular momentum of magnetization and that of the incident spins must be conserved, i.e., the total torque

$\boldsymbol{T} = \mathrm{d}\boldsymbol{L}/\mathrm{d}t = 0$. Therefore $\boldsymbol{T}_\mathrm{e} + \boldsymbol{T}_\mathrm{M} = 0$, where $\boldsymbol{T}_\mathrm{e}$ is the torque acting on the ensemble of incident spin-polarized electrons and $\boldsymbol{T}_\mathrm{M}$ is the torque exerted in turn on the magnetization. Consequently, by determining $\boldsymbol{T}_\mathrm{e}$ experimentally, we have also measured $\boldsymbol{T}_\mathrm{M}$. From $\boldsymbol{T}_\mathrm{M}$, we can then calculate the Larmor frequency ω_M of the magnetization and determine the conditions for precessional magnetization reversal (see Sect. 3.2). In the following discussion, we have to distinguish between the experiments in transmission and reflection geometry.

What is observed in the transmission experiments is the angle ϵ by which the spin-polarization vector of the ensemble of injected electrons has precessed on traversing the ferromagnetic film of thickness d without losing energy. According to the discussion in the preceding section, linear thickness dependence of the precession angle is expected and observed: $\epsilon(d) = \tilde{\epsilon} d$. With the precession frequency $\omega_\mathrm{e} = \tilde{\epsilon} v$ and the current density $j = n_\mathrm{e} e v$ of the transmitted electrons, where n_e is the electron density, the torque (per unit volume) acting on the injected spins is $T_\mathrm{e} = |\boldsymbol{\omega}_\mathrm{e} \times \boldsymbol{L}_\mathrm{e}| = P_0 n_\mathrm{e} \omega_\mathrm{e} (\hbar/2) \sin\vartheta = (\hbar/2e) P_0 j \tilde{\epsilon} \sin\vartheta$. All quantities determining T_e are thus determined by the experiment without any further assumptions. On the other hand, the torque (per unit volume) acting on the magnetization is $T_\mathrm{M} = |\boldsymbol{\omega}_\mathrm{M} \times \boldsymbol{L}_\mathrm{M}| = \omega_\mathrm{M} L_\mathrm{M} \sin\vartheta$. With $T_\mathrm{M} = T_\mathrm{e}$, the precession frequency of $\boldsymbol{M}$ is then obtained from

$$\omega_\mathrm{M} = \frac{P_0 \cdot j \cdot \tilde{\epsilon}}{e \cdot n_\mathrm{M} \cdot n_\mathrm{B}}\,, \tag{1}$$

where n_M is the density of the atoms in the ferromagnet. For simplicity, we have neglected the orbital contribution to magnetization by setting the angular momentum (per unit volume) $L_\mathrm{M} = n_\mathrm{B} n_\mathrm{M} \hbar/2$. Again, all quantities entering (1) can be measured directly.

Besides a precession, there is simultaneously a rotation of the spin-polarization vector into the direction of $\boldsymbol{M}$. This motion of $\boldsymbol{P}$ is characterized by spin asymmetry A, as discussed in the preceding section. It generates a component $P_{||}$ of the spin-polarization vector parallel to $\boldsymbol{M}$. There is no torque generated in this process. But as $P_{||}$ increases, M must decrease to conserve the magnitude of the total angular momentum. The subsequent recovery of the magnitude of M to its thermodynamic equilibrium involves localized and traveling spin waves and is not considered here.

Note that $\boldsymbol{M}$ relaxes also into $\boldsymbol{P}$. However, this relaxation is much slower than the relaxation of $\boldsymbol{P}$ into $\boldsymbol{M}$ which takes only few femtoseconds. The relaxation time of $\boldsymbol{M}$ into the direction of a magnetic field is obtained from experiments determining the damping parameter in the Landau–Lifshitz–Gilbert equation [39], from the width of the ferromagnetic resonance, or directly by time-resolved images of the magnetization precession [9,40]. The relaxation time of $\boldsymbol{M}$ into the direction of an applied magnetic field turns out to be of the order of several 100 ps [41,42]. In thin films, it is mainly due to the excitation of spin waves. This explains why the relaxation of $\boldsymbol{M}$ is

so much slower than the relaxation of $\boldsymbol{P}$ into $\boldsymbol{M}$ which is caused by spin-dependent electron absorption.

In reflection, a significant torque is exerted on the magnetization only within the surface region of the ferromagnet, so that (1) has to be modified. First, j is now the density of the reflected current, and second, the specific precession angle $\tilde{\epsilon}$ has to be replaced by the ratio ϵ/λ where λ is the inelastic mean free path.

3.2 Precessional Magnetization Reversal

Recently, it has been shown that picosecond magnetic field pulses of surprisingly small amplitudes can induce magnetization reversal in thin in-plane magnetized, uniaxial films [39]. The fact that the external magnetic field pulse $\boldsymbol{B}_{\text{ext}}$ is applied in the plane of the film at a right angle to $\boldsymbol{M}$ is crucially important (see Fig. 16). In this way, maximum torque is exerted on the magnetization leading to a precession of $\boldsymbol{M}$ about $\boldsymbol{B}_{\text{ext}}$ out of the plane of the film. As $\boldsymbol{M}$ leaves the plane of the film, the demagnetizing field $\boldsymbol{B}_{\text{demag}}$ comes into play. It increases with the angle ϵ_{M} between $\boldsymbol{M}$ and the film plane, $B_{\text{demag}} \sim \sin\epsilon_{\text{M}}$. When the external magnetic field pulse ceases to exist, $\boldsymbol{B}_{\text{demag}}$ still persists, and $\boldsymbol{M}$ continues to precess now about $\boldsymbol{B}_{\text{demag}}$ (plus the anisotropy field). Finally, $\boldsymbol{M}$ relaxes into one of the two easy directions of magnetization (not shown in Fig. 16). Thus, to trigger precessional magnetization reversal in in-plane magnetized films, the magnetization must precess out of plane by a certain angle, which is determined by $\boldsymbol{B}_{\text{demag}}$, the

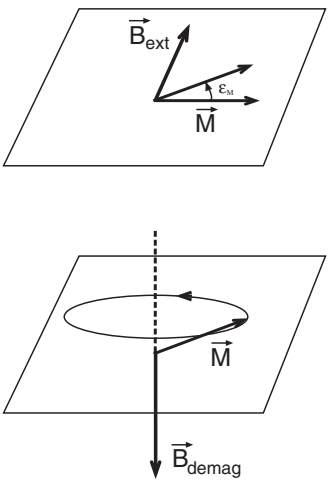

Fig. 16. Precessional magnetization switching. *Top*: The magnetization $\boldsymbol{M}$ precesses out of the plane by an angle ϵ_{M} under the action of the external magnetic field $\boldsymbol{B}_{\text{ext}}$ which is in the plane at a right angle to $\boldsymbol{M}$. *Bottom*: The magnetization precesses about the demagnetizing field $\boldsymbol{B}_{\text{demag}}$

anisotropy field, and the damping constant. Using typical values for these parameters [39], a precession angle $\epsilon_{\mathrm{M}} \approx 20^{\circ}$ of magnetization is needed.

3.2.1 By a Regular Magnetic Field

The time for the elementary process of magnetization reversal is given by the Larmor precession in the anisotropy field. Therefore, picosecond pulses of sufficient strength are needed. Such magnetic field pulses are produced in the Final Focus Test beam facility of the Stanford Linear Accelerator Center, where a pulsed electron beam of ≈ 1000 A can be focused on an area of several $\mu\mathrm{m}^2$ [43]. The magnetic field pulses generated in the target are unique because they combine short duration of a few picoseconds with strength that depends on the distance from the center but reaches values as large as 20 T.

After exposing a ferromagnetic sample to such extreme field pulses, the sample is removed from the beam, and the recorded magnetization pattern is imaged by a spin-polarized scanning electron microscope [44]. As an example, Fig. 17 shows the magnetization pattern generated by one electron pulse of 4.4 ps duration (through the center of the image) in a uniaxial Co film [39]. Before exposure, the film had been premagnetized to the right. In the dark regions, the magnetization has switched to the left. The largest diameter of the pattern is 225 µm. There is, of course, beam damage, but it is hardly visible on the scale of this figure. The outer boundary of the pattern can readily be understood by the conservation of angular momentum. This figure-eight pattern approximates the contour line of constant nonvanishing torque $\boldsymbol{T} = \text{const}$. When $\boldsymbol{B}_{\mathrm{ext}}$ is perpendicular to $\boldsymbol{M}$, T is largest, i.e., reversal occurs furthest away from the center, in fact at locations with surprisingly low fields [39]. However, if $\boldsymbol{B}_{\mathrm{ext}}$ is parallel or antiparallel to $\boldsymbol{M}, T = 0$, and

Fig. 17. The magnetization pattern recorded in a 20-nm thick uniaxial Co/Pt/MgO(110) film, which has been written by one pulse of 4.4 ps duration. The image area is 300 µm × 300 µm. The magnetization in the bright regions is still pointing along the original direction, but it has switched to the opposite direction in the dark regions

no reversal occurs even in the immense fields close to the center of the beam. This proves that picosecond field pulses of sufficient strength can trigger precessional magnetization reversal.

The white regions following the first reversal indicate where back reversal has occured, i.e., where $\boldsymbol{M}$ has precessed by more than 180° about the demagnetizing field. The subsequent dark regions mean double reversal, i.e., $\boldsymbol{M}$ has precessed by more than 360° about the demagnetizing field. At distances still closer to the center, multiple reversals and back reversals follow each other so closely in space that they annihilate each other in the slow thermal relaxation process following the beam pulse.

3.2.2 By the Exchange Field

May precessional magnetization reversal also be feasible with picosecond exchange field pulses? To answer this question, (1) has to be considered. Assuming an electron current which is completely spin-polarized perpendicularly to $\boldsymbol{M}$ ($P_0 = 1$) and a current density of $j = 10^{13}$ Am^{-2}, which has been realized in nanocontacts [4,45], we find that pulse durations of a few picoseconds are sufficient to induce precessional magnetization reversal. Injection of such a pulse of spin-polarized electrons is equivalent to applying a magnetic field pulse of an amplitude of roughly 1 T for all three ferromagnets Fe, Co, and Ni. It is emphasized that the choice of a smaller current density j and hence a smaller Larmor frequency ω_{M} can be compensated for by a larger pulse duration, yet only as long as this latter value remains much smaller than the spin-lattice relaxation time, which is of the order of several hundred picoseconds [41,42].

From the technological point of view, the most appropriate electron energy is the Fermi energy E_{F}. However, so far, the precession angle ϵ has not been measured at energies below vacuum energy. There is no principal obstacle to using an all-solid-state device with two ferromagnetic films before and after the sample under investigation; one film acts as a source, and the other as a detector of spin polarization [46]. On the basis of the spin-polarized band structure of the ferromagnetic metals, it is very likely that the exchange energy and hence $\tilde{\epsilon}$ will increase on approaching E_{F}. This will make it even easier to induce precessional magnetization reversal by injecting spin-polarized electrons.

It is emphasized that the axis of precession of $\boldsymbol{M}$ changes direction in space as the injected electrons travel through the ferromagnet. This arises, because the torque $\boldsymbol{T}_{\mathrm{e}} = -\boldsymbol{T}_{\mathrm{M}}$ is always perpendicular to $\boldsymbol{M}$ and $\boldsymbol{P}$; hence, the axis of precession changes direction with the precession of $\boldsymbol{P}$. Yet, to use the torque $\boldsymbol{T}_{\mathrm{M}}$ for precessional magnetization reversal, there has to be a preferred direction in the crystal lattice about which the magnetization must precess. This can be achieved by making the ferromagnetic film thin enough. The experiments described in Sect. 2.4 show that the precession of $\boldsymbol{P}$ may be neglected altogether if the magnetically active part of the film

is about 1 nm thick. In reflection geometry, on the other hand, the condition of a thin sample for obtaining uniform precession of $\boldsymbol{M}$ is automatically met by the limited penetration depth of the electrons.

Until now, we have not considered the effect of the regular magnetic field which is always induced by an electric current. Hence the question arises whether the regular magnetic field and the exchange field are of comparable strength. A simple calculation proves that the precession due to the exchange field is always faster compared to that of the regular magnetic field as soon as one injects the current through a nanocontact. The maximum field strength $B_{\max}$ of a current flowing across a circular area with radius r is given by $B_{\max} = \mu_0 jr/2$ (μ_0: vacuum permeability) and induces a precessional motion of the magnetization with frequency $\omega_{\max} = (e/m)B_{\max}$. Hence, precession due to the exchange field dominates over the precession induced by the regular magnetic field, if

$$\frac{\omega_{\max}}{\omega_{\mathrm{M}}} = \frac{\mu_0 e^2}{2m} \cdot \frac{n_{\mathrm{M}} n_{\mathrm{B}} r}{P_0 \tilde{\epsilon}} < 1\,. \tag{2}$$

Given the fact that $\tilde{\epsilon}/n_{\mathrm{B}}$ as well as n_{M} do not vary much with the different 3 d ferromagnets, this situation is realized if the radius r of the nanocontact is smaller than 100 nm.

4 Conclusion

Electrons whose spin polarization vector is perpendicular to the magnetization direction have been spin analyzed after transmission through a ferromagnetic layer, respectively, reflection from a ferromagnetic surface. The incident spin wave function is a coherent superposition of a spin wave function with its spin parallel to $\boldsymbol{M}$ and one with its spin antiparallel to it. Due to different phase factors and amplitudes of the two spin functions, which are caused by the exchange energy and the inelastic spin-dependent scattering in the ferromagnet, two types of motion of the spin-polarization vector occur: a precession about $\boldsymbol{M}$ and a rotation into it. It is shown how the torque generated on magnetization by incident spin-polarized electrons can be determined by exploiting the law of angular momentum conservation. Precessional magnetization reversal by injecting spin-polarized electrons is proposed as a new concept for magnetization reversal.

References

1. J. C. Slonczewski: Current-driven excitation of magnetic multilayers, J. Magn. Magn. Mater. **159**, L1 (1996)
2. L. Berger: Emission of spin waves by a magnetic multilayer traversed by a current, Phys. Rev. B **54**, 9353 (1996)

3. Ya. B. Bazaliy, B. A. Jones, Shou-Cheng Zhang: Modification of the Landau–Lifshitz equation in the presence of a spin-polarized current in colossal- and giant-magnetoresistive materials, Phys. Rev. B **57**, R3213 (1998)
4. M. Tsoi, A.G.M. Jansen, J. Bass, W.-C. Chiang, M. Seck, V. Tsoi, P. Wyder: Excitation of a magnetic multilayer by an electric current, Phys. Rev. Lett. **80**, 4281 (1998)
5. E. B. Myers, D. C. Ralph, J. A. Katine, R. N. Louie, R. A. Buhrman: Current-induced switching of domains in magnetic multilayer devices, Science **285**, 867 (1999)
6. J. Z. Sun: Current-driven magnetic switching in manganite trilayer junctions, J. Magn. Magn. Mater. **202**, 157 (1999)
7. J.-E. Wegrowe, D. Kelly, Y. Jaccard, Ph. Guittienne, J.-Ph. Ansermet: Current-induced magnetization reversal in magnetic nanowires, Europhys. Lett. **45**, 626 (1999)
8. M. Tsoi, A. G. M. Jansen, J. Bass, W.-C. Chiang, V. Tsoi, P. Wyder: Generation and detection of phase-coherent current-driven magnons in magnetic multilayers, Nature **406**, 46 (2000)
9. Y. Acremann, M. Buess, C. H. Back, M. Dumm, G. Bayreuther, D. Pescia: Ultrafast generation of magnetic fields in a Schottky diode, Nature **414**, 51 (2001)
10. W. Weber, S. Riesen, H. C. Siegmann: Magnetization precession by hot spin injection, Science **291**, 1015 (2001)
11. M. N. Baibich, J. M. Broto, A. Fert, F. Nguyen Van Dau, F. Petroff, P. Etienne, G. Creuzet, A. Friederich, J. Chazelas: Giant magnetoresistance of (001)Fe/(001)Cr magnetic superlattices, Phys. Rev. Lett. **61**, 2472 (1988)
12. T. Valet, A. Fert: Theory of the perpendicular magnetoresistance in magnetic multilayers, Phys. Rev. B **48**, 7099 (1993)
13. N. F. Mott, H. Jones: *The Theory of the Properties of Metals and Alloys* (Clarendon Press, Oxford 1936)
14. D. P. Pappas, K.-P. Kämper, B. P. Miller, H. Hopster, D. E. Fowler, C. R. Brundle, A. C. Luntz, Z.-X. Shen: Spin-dependent electron attenuation by transmission through thin ferromagnetic films, Phys. Rev. Lett. **66**, 504 (1991)
15. G. Schönhense, H. C. Siegmann: Transmission of electrons through ferromagnetic material and applications to detection of electron spin polarization, Ann. Physik **2**, 465 (1993)
16. Y. Lassailly, H.-J. Drouhin, A. J. van der Sluijs, G. Lampel, C. Marlière: Spin-dependent transmission of low-energy electrons through ultrathin magnetic layers, Phys. Rev. B **50**, 13054 (1994)
17. D. Oberli, R. Burgermeister, S. Riesen, W. Weber, H. C. Siegmann: Total scattering cross section and spin motion of low energy electrons passing through a ferromagnet, Phys. Rev. Lett. **81**, 4228 (1998)
18. Note that precession of the electron spin-polarization vector caused by elastic exchange scattering as proposed by J. Byrne and P. S. Farago [Faraday rotation of electron spin polarization, in J. Phys. B **4**, 954 (1971)] can be neglected. As is shown in Sect 2.4, elastic exchange scattering can be of only minor importance in our experiments
19. H. A. Tolhoek: Electron polarization, theory and experiment, Rev. Mod. Phys. **28**, 277 (1956)

20. V. Grolier, J. Ferré, A. Maziewski, E. Stefanowicz, D. Renard: Magneto-optical anisometry of ultrathin cobalt films, J. Appl. Phys. **73**, 5939 (1993)
21. M. P. Seah, W. A. Dench: Quantitative electron spectroscopy of surfaces: A standard data base for electron inelastic mean free paths in solids, Surf. Interface Anal. **1**, 2 (1979)
22. H. J. Drouhin, A. J. van der Sluijs, Y. Lassailly, G. Lampel: Spin-dependent transmission of free electrons through ultrathin cobalt layers, J. Appl. Phys. **79**, 4734 (1996)
23. O. Paul: Dissertation ETH No. 9210 (1990)
24. C. Marlière, D. Renard, J.-P. Chauvineau: Study of interface roughness and crystallographic structure of Au/Co/Au sandwiches, Thin Solid Films **201**, 317 (1991)
25. W. Weber, A. Bischof, R. Allenspach, C. H. Back, J. Fassbender, U. May, B. Schirmer, R. M. Jungblut, G. Güntherodt, B. Hillebrands: Structural relaxation and magnetic anisotropy in Co/Cu(001) films, Phys. Rev. B **54**, 4075 (1996)
26. H. C. Siegmann: *Selected Topics on Electron Physics*, D. M. Campbell, H. Kleinpoppen (Eds.) (Plenum, New York 1996)
27. M. P. Gokhale, D. L. Mills: Origin of spin-dependent asymmetries in electron transmission through ultrathin ferromagnetic films, Phys. Rev. Lett. **66**, 2251 (1991)
28. M. Aeschlimann, M. Bauer, S. Pawlik, W. Weber, R. Burgermeister, D. Oberli, H. C. Siegmann: Ultrafast spin-dependent electron dynamics in fcc Co, Phys. Rev. Lett. **79**, 5158 (1997)
29. The work function of the Co(001) surface was reduced by adsorption of small amounts of cesium
30. We note that nonuniformity of the ferromagnetic film thickness results in larger d_0 values in the electron experiment compared to those obtained from the magneto-optic Kerr effect. The values of the specific precession angle $\tilde{\epsilon}$, however, are not affected by this
31. E. Colavita, M. De Crescenzi, L. Papagno, R. Scarmozzino, L. S. Caputi, R. Rosei, E. Tosatti: Single-particle and collective excitations in ferromagnetic iron from electron-energy-loss spectroscopy, Phys. Rev. B **25**, 2490 (1982)
32. R. Feder: Spin-polarised low-energy electron diffraction, J. Phys. C **14**, 2049 (1981)
33. T. Duden, E. Bauer: Spin-polarized low energy electron microscopy, Surf. Rev. Lett. **5**, 1213 (1998)
34. D. Tillmann, R. Thiel, E. Kisker: Very-low-energy spin-polarized electron diffraction from Fe(001), Z. Phys. B **77**, 1 (1989)
35. The phase shift has been discussed in the literature only for an absolute band gap [see for instance J. B. Pendry, S. J. Gurman: Theory of surface states: General criteria for their existence, Surf. Sci. **49**, 87 (1975)], but this statement is still true for a relative band gap, at least for a certain portion of the reflected electrons
36. A. Shorikov, V. I. Anisimov: private communication
37. It is emphasized that the thickness dependence of ϵ should not follow a simple exponential law because of its accumulative character. Instead, $\epsilon(d)$ at 9 eV is analyzed using the following expression: $\epsilon(d) \sim (\int_0^{\alpha d} y\mathrm{e}^{-y/\lambda}\mathrm{d}y)/(\int_0^{\alpha d} \mathrm{e}^{-y/\lambda}\mathrm{d}y) = \lambda+\alpha d/(1-\mathrm{e}^{\alpha d/\lambda})$ with $\alpha = 2/\cos 45^\circ$, taking into account our particular experimental geometry

38. S. F. Cheng, V. G. Harris, G. A. Prinz: Dependency of coercivity on Co layer thickness in Co/Cu multilayer structures, IEEE Trans. Magn. **33**, 3529 (1997)

39. C. H. Back, R. Allenspach, W. Weber, S. S. P. Parkin, D. Weller, E. L. Garwin, H. C. Siegmann: Minimum field strength in precessional magnetization reversal, Science **285**, 864 (1999)
40. Y. Acremann, C. H. Back, M. Buess, O. Portmann, A. Vaterlaus, D. Pescia, H. Melchior: Imaging precessional motion of the magnetization vector, Science **290**, 492 (2000)
41. A. Vaterlaus, T. Beutler, D. Guarisco, M. Lutz, F. Meier: Spin-lattice relaxation in ferromagnets studied by time-resolved spin-polarized photoemission, Phys. Rev. B **46**, 5280 (1992)
42. A. Scholl, L. Baumgarten, R. Jacquemin, W. Eberhardt: Ultrafast spin dynamics of ferromagnetic thin films observed by femtosecond spin-resolved two-photon photoemission, Phys. Rev. Lett. **79**, 5146 (1997)
43. H. C. Siegmann, E. L. Garwin, C. Y. Prescott, J. Heidmann, D. Mauri, D. Weller, R. Allenspach, W. Weber: Magnetism with picosecond field pulses, J. Magn. Magn. Mater. **151**, L8 (1995)
44. R. Allenspach: Ultrathin films: Magnetism on the microscopic scale, J. Magn. Magn. Mater. **129**, 160 (1994)
45. N. Garcia, H. Rohrer, I. G. Saveliev, Y.-W. Zhao: Negative and positive magnetoresistance manipulation in an electrodeposited nanometer Ni contact, Phys. Rev. Lett. **85**, 3053 (2000)
46. L. Berger: Precession of conduction-electron spins near an interface between normal and magnetic metals, IEEE Trans. Magn. **31**, 3871 (1995)